Second-order phase transition in $FeCr_2S_4$ investigated by Mössbauer spectroscopy: An example of orbital para-to-ferromagnetism transition

L. Brossard, J. L. Dormann, L. Goldstein, P. Gibart, and P. Renaudin
Laboratoire de Magnétisme, Centre National de la Recherche Scientifique, 1 place Aristide Briand, 92190 Bellevue, France
(Received 19 April 1978)

Mössbauer studies on stoichiometric samples of the spinel ferrimagnet $FeCr_2S_4$ are reported with special attention to the second-order phase transition at 13 K. Magnetic spectra were first solved as a superposition of singlets. This gives the experimental linewidths and intensities of each line. These as-deduced linewidths and intensities were assumed in computing the magnetic spectra for a single-site solution. The transition at 13 K is associated to a discontinuity of the barycenter of the spectra. Moreover, anomalies of the linewidth variations versus T as well as differences between the theoretical and the experimental intensities of the peaks cannot be resolved in the single-site solution. The singleness of this solution is discussed. A more reliable two-site solution is suggested. The experimental mean linewidth, the characteristics of the electric-field-gradient (EFG) (V_{zz}, η, and θ), and the hyperfine magnetic field of the sites show discontinuities at 13 K. These features are explained assuming narrow d bands in $FeCr_2S_4$. The sixth $3d$ electron of A-site Fe^{2+} is assumed to occupy an orbital with $|\epsilon\rangle$ and $|\theta\rangle + |\psi_{Cr^{2+}}\rangle$ symmetry due to the hybridization of $|\theta\rangle$ with the B-site Cr^{2+} state. Fe_A^{2+} and Cr_B^{2+} in thiospinel lie almost at the same energy level. At $T > 13$ K, the sixth $3d$ electron shares the $|\epsilon\rangle$ and the hybridized $|\theta\rangle$ orbital statistically. This gives two sites with the same intensity. At $T < 13$ K, only the hybridized $|\theta\rangle$ orbital is occupied. This corresponds to an orbital paramagnetism ($T > 13$ K) to a ferromagnetic ordering ($T < 13$ K) transition. Recently Cyrot showed that an Hubbard Hamiltonian in the atomic limit leads not only to spin ordering but also to orbital ordering. Furthermore, the transition at $T < 13$ K is associated to a slow relaxation of the EFG. The coupling of the band with the phonons at $T < 13$ K is different from a linear and weak dynamic Jahn-Teller effect as is the case for A-site diluted Fe^{2+}.

I. INTRODUCTION

A. General introduction

Since 1956,[1] the ferrimagnetic normal spinel $FeCr_2S_4$ has been studied in a large number of crystallographic, magnetic, and electric investigations as well as by Mössbauer spectroscopy.

On both sides of the Curie temperature ($T_C = 177$ K), Eibschutz *et al.*[2] have interpreted their Mössbauer spectra assuming an electric-field gradient (EFG) induced by the magnetic order. At low temperature (13 K) there appears a λ anomaly in the specific heat,[3] which affects strongly the Mössbauer spectra: a static to dynamic Jahn-Teller transition was proposed by Spender and Morrish.[4] Later on, an antidistorsive transition was hypothesized by Van Diepen and Van Stapele[5] to explain this second-order phase transition.

No explanation given so far is completely consistent with experimental results. This will be discussed in Sec. II, where the previous interpretations of $FeCr_2S_4$ Mössbauer spectra related to a single-A-site Fe^{2+} are reviewed.

We have reinvestigated this transition by Mössbauer spectroscopy using a very well-defined sample. It has been shown previously that departures from the stoichiometric composition[3] smooth the λ transition. Therefore our experiments were carried out on a stoichiometric sample which exhibits the smallest linewidth reported so far. The main problem was to understand the nature of the second-order transition at 13 K.

Mössbauer spectroscopy was chosen as the best tool to study the electronic structure of iron atoms and departures from T_d local symmetry. Other methods were used too (magnetization, low-temperature x-ray diffraction, neutron diffraction, and transport properties) but the informations obtained by these methods give only macroscopic results.

The transition has been recognized as an orbital paramagnetism to an orbital ferromagnetism one by analogy with the orbital para-to-antiferromagnetism transition theoretically studied by Cyrot *et al.*[6] Our Mössbauer results are strongly supported by such a

model which describes the sixth $3d$ electron of A-site Fe^{2+} in a narrow band hybridized with the B-site Cr^{2+} states (Sec. IV). This description is justified by the low mobility of the p-type carriers. A single-ion crystal-field theory does not rigorously describe the transport and magnetic properties of $FeCr_2S_4$.

The physical properties of $FeCr_2S_4$ are first reviewed in Sec. I B.

In Sec. III, our Mössbauer experimental results are presented with a first reproduction based on a single-A-site Fe^{2+}. The singleness of this solution is discussed and an improved interpretation of the spectra is obtained by superposing two types of A-site Fe^{2+}. These two sites correspond to the occupation of the two orbitals, x^2-y^2 and B-site-Cr^{2+} hybridized $3z^2-r^2$.

B. Physical properties of $FeCr_2S_4$

The compound is a cubic normal spinel whose room-temperature unit-cell parameter a,[7] and anion shift parameter u,[8] are, respectively, 9.995 Å and 0.385 ($u > \frac{3}{8}$). The S-S distance is 3.5 Å whereas the ionic and covalent sulfur radii are 1.84 and 1.02 Å, respectively. Low-temperature ($T = 77$,[9] 5,[5] and[10] 4.2 K) x-ray measurements led to the conclusion of the absence of any cubic to tetragonal transformation contrary to what is observed in $FeCr_2O_4$ at $T = 120$ K.[11]

$FeCr_2S_4$ is a p-type ferrimagnetic semiconductor[12,13]

$$p \sim (1-2)\times 10^{19}\ \text{cm}^3;\quad \mu_p \sim 0.2-0.3\ \text{cm}^2/\text{V sec}\ .^{14}$$

(p is the carrier concentration, μ_p is the mobility of holes, and K_1 is the anisotropy constant.) A single-electron narrow-d-band description of the transport properties is more consistent than the crystal-field approach.[15] The magnetic moment at 4.2 K is 1.6 μ_B[16] $K_1(>0) = 3\times 10^6$ erg/cm^3 at 4.2 K (about 2 cm^{-1}/Fe^{2+}).[16,17] $K_1(T)$ follows the power law $K_1(T) \propto (M/M_0)^{10}$. Neutron-diffraction data[8] account for the antiparallel coupling[18] of the resultant spin of A-site Fe^{2+} (4.2 μ_B) and B-site Cr^{3+} (2.9 μ_B).

Specific-heat data[3] show a λ peak near 10 K, characteristic of a second-order phase transition: this excludes any crystallographic transformation since they present the characteristic specific-heat discontinuity of the first-order phase transition.

Departures from stoichiometry in $FeCr_2S_4$ were systematically studied by Mössbauer spectroscopy and relevant transport and magnetic properties.[19,20]

II. CRITICAL REVIEW OF PREVIOUS STUDIES

(i) The first study is due to Eibschutz *et al.* who tentatively interpret their results on the basis of single-ion crystal-field theory.

At $T > T_C$, the second-order spin-orbit coupling splits the ^5E ground state of T_d-local-symmetry Fe^{2+} into five equally spaced levels: a singlet A_1, a doublet E, a triplet T_1,...; the distance K between them is[21]

$$K = 6\left(\frac{\lambda^2}{\Delta} + \rho\right),$$

where Δ is the crystal-field splitting of $3d^6$ configuration in a regular tetrahedral symmetry, and λ and ρ are the spin-orbit and spin-spin coupling parameters. The mean value of the principal component V_{ZZ} of the electric-field gradient (EFG) vanishes on each of these levels in the case of a rapid electronic relaxation; at high temperature a zero quadrupole interaction results and hence a singlet.

At $T < T_C$, the magnetic order splits the ^5E level into five orbital doublets whose residual degeneracy is lifted by second-order spin-orbit coupling[22,23]: then, the mean value of V_{ZZ} does not vanish and the thermal average of V_{ZZ} leads one to observe a quadrupole interaction in the presence of an hyperfine magnetic field. The EFG is therefore induced by the magnetic order; it has been also observed in the B-site Fe^{2+} of $RbFeF_3$,[24] and theoretically interpreted by Ganiel *et al.*[25] This interpretation agrees fairly well with the experimental spectra obtained at $T > 22$ K.

The EFG induced by magnetic order is positive ($V_{ZZ} > 0$), axial ($\eta = 0$) and the principal Z axis of the EFG is parallel to the easy axis of magnetization directed along [100] ($\theta = 0$, where θ is the angle between Z and the spin direction z in the XYZ principal axis system of the EFG).

Nevertheless, this interpretation is not entirely consistent. Assuming

$$eQV_{ZZ}(T=0) = 3\ \text{mm/sec}\ ,$$

Eibschutz *et al.* deduced that $K = 5$ cm^{-1} and $\lambda = 60$ cm^{-1} from the temperature dependence of H and V_{ZZ}. These values seem to be low compared to those obtained in A-site Fe^{2+} in some sulfide compounds.[21] In these systems, Fe^{2+} ions are diluted and the crystal-field theory is a good approximation. The reliable value of 12 cm^{-1} for K was obtained with

$$\lambda \sim 60\ \text{cm}^{-1},\ \Delta \sim 2400\ \text{cm}^{-1}\ ,$$

and

$$\rho \sim 0.5\ \text{cm}^{-1}$$

and the calculated temperature dependence of H and V_{ZZ} agrees well with the experimental results on $CdCr_2S_4$:^{57}Fe.[22,23] They differ from the $FeCr_2S_4$ data: for example, at low temperatures, the orbital reduction of H at $T/T_C = 0.125$ is 8% in $FeCr_2S_4$ against 55% in $CdCr_2S_4$:^{57}Fe (cf. Fig. 1).

Moreover, an Heisenberg Hamiltonian does not

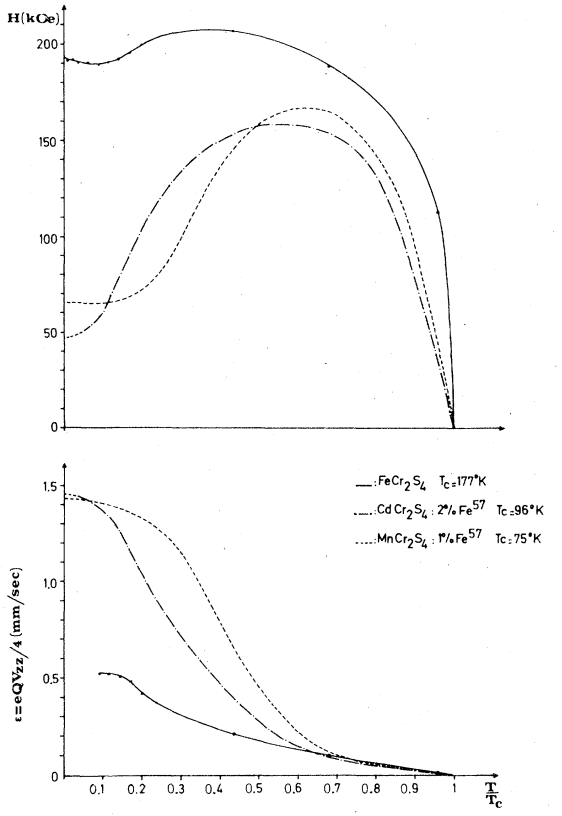

FIG. 1. Variation with temperature of the hyperfine magnetic field H and of the principal component V_{zz} of the EFG for $FeCr_2S_4$ in a single-site solution (present work), $CdCr_2S_4$: 2-at.% ^{57}Fe from Ref. 23, and $MnCr_2S_4$: 1-at.% ^{57}Fe (Ref. 26).

rigorously describe the exchange interactions[27] acting on the ^5E ground state of Fe^{2+} A.

(ii) Hoy *et al.*[28] found for $T < T_C$

$$V_{ZZ} < 0 \text{ and } \theta = \pi/2 \text{ for } 61\text{ K} < T < T_C ,$$

$$\eta = 0 \text{ for } 121\text{ K} < T < T_C ,$$

and

$$\eta = 0.8 \text{ for } T = 61\text{ K} .$$

They concluded that the EFG which appears below T_C is primarily due to a temperature-dependent lattice distortion associated with magnetostrictive effects.

(iii) In 1972, Spender and Morrish[4,29] used polycrystalline powders mixed with some glue or transoptic powder.

At $T > 10$ K, the variations of the hyperfine parameters H and V_{ZZ} agree with Eibschutz's results. H is minimum near $T = 10$ K; V_{ZZ} and θ present some discontinuities around 10 K: At $T < 10$ K, V_{ZZ} becomes negative ($eQV_{ZZ} = -5.30$ mm/sec at $T = 4.4$ K) and $\theta = \frac{1}{2}\pi$ with $\eta \sim 0.20$.

Spender and Morrish found[4] that all the linewidths in a given spectrum are not the same. Furthermore, their fitting shows clearly that the normalized experimental intensities of the peaks are not equal in a given spectrum to the theoretical one as they can be deduced from the values of H, V_{ZZ}, η, θ, and ϕ.[30]

In order to explain these features, Spender and Morrish consider the conjugated effects of:

(a) a relaxation between ferrous and ferric behavior in relation with the increasing mobility of carriers in the A-site Fe^{2+} narrow band when T decreases at high T.

(b) a dynamic Jahn-Teller (JT) effect with a temperature-dependent relaxation rate ω_{JT}, leading at $T > T_C$ to the Mössbauer singlet.[31]

(c) a low-temperature A-site trapping leading at $T < T_C$ to the observed quadrupole interaction whose magnitude depends on ω_{JT}: the low value of V_{ZZ} at 14 K has been attributed to such a dynamic JT effect.

In our opinion such a reduction of V_{ZZ} is too important to be related to a dynamic JT effect which is known to be linear and weak for A-site Fe^{2+}.[32,33] In such a case, the Ham reduction factor q[34,35] is close to 1. Moreover, $\frac{1}{2} < q < 1$ for a linear dynamic JT effect. Even in the case of a strong quadratic (or anisotropic) dynamic JT effect,[36,37] $q \lesssim \frac{1}{2}$. Now, in the present case, the reduction factor is nearly equal to 0.4 (cf. Fig. 1), which excludes any dynamic JT effect. Such an effect should reduce to a static one at lower temperatures. In a concentrated JT ion system, this should lead to a cooperative transition with a cubic to tetragonal crystallographic transformation such as in $FeCr_2O_4$.[38]

(iv) Van Diepen and Van Stapele[5] obtained experimental data on $FeCr_2S_4$ in agreement with those of Spender and Morrish, then tried to fit their results at $T > 20$ K (where $\eta = 0$) on the basis of the static-crystal-field theory describing the EFG induced by the magnetic order. Although the Ham reduction factor q could be lower in $FeCr_2S_4$ than in diluted iron thiospinels,[5,16] they suggest that a negative coupling between local JT distortions may be the origin of the weaker temperature dependence of V_{ZZ}. This negative interaction between the sites of the two Bravais tetrahedral sublattices should give rise to a cooperative distortion of A sites. In a molecular-field approximation and for nearest-neighbor interactions only, they obtained a critical temperature T_{crit}. They found that H and $V_{ZZ}(= V_{XX}$, component of the EFG directed along H) are constants at $T < T_{crit} = 20$ K. The experimental value suggests a lower $T_{crit}(\sim 13$ K) of this "antiferrodistorsive" transition.

Finally, it should be noted that this model does not take into account the excited state of Cr^{3+} B which plays an important role in the transport properties of $FeCr_2S_4$.

III. EXPERIMENTAL RESULTS

A. Methodology

The sample has been prepared from the elements (iron and chromium 99.999% and sulfur 99.9999%) and a single spinel phase has been obtained after several firings at 1000 °C and grinding.

The polycrystal absorber powder contains 10 mg Fe/cm^2 and is finely mixed with rilsan powder: the whole thing is cold-pressed between two aluminum-Mylar foils without any iron impurity. Thus, we avoid the use of glue since A-site Fe^{2+} is known to be sensible at low temperatures to quadrupole interactions induced by glue strains.[39]

Paramagnetic spectra are singlets whose experimental linewidths Γ_{ex} are, respectively, 0.30 and 0.27 mm/sec at 200 K and at room temperature. This shows that our compound is close to the stoichiometric composition $FeCr_2S_4$ and characterized by a very low A-site Fe^{3+} and B-site vacancy content.[19,20]

The magnetic spectra require some comments on the programmation method used: they were fitted using a least-squares routine based on the convolution of Lorentzian emission and absorption lines whose linewidths are, respectively, Γ_s and $\nu_a\Gamma_s$.[19,40] Then, the mean linewidth Γ_{ex} can be expressed by

$$\Gamma_{ex}=\Gamma_s(1+\nu_a)(1+0.125\,t)\ , \qquad (1)$$

where t is the Mössbauer effective thickness of the sample. It can be seen[19,40] that this expression is a better approximation of Γ_{ex} for $t<1$ than the formula suggested by Wisscher[41] for $t<5$. When computing the magnetic spectra, t has been supposed to be constant although f' and then t increase when the temperature is lowered. This affects only the total absorption area of the spectra and not the relative intensities β_i of the peaks of each spectrum. These β_i are equal to the nuclear transition probabilities. They are calculated by a subroutine from the peak's positions and then from the values of the hyperfine parameters H, V_{ZZ}, η, θ, and ϕ. The program used can introduce fixed β_i values different from the calculated one. It is possible to use as parameter, regardless of β_i, the linewidth Γ_i of the ith peak ($i_{max}=6$ or 8) through the broadening factor ν_i

$$\Gamma_i=\Gamma_{ex}(1+\nu_a\nu_i)/(1+\nu_a)\ . \qquad (2)$$

In a first step (Sec. III B) each magnetic spectrum has been solved as a superposition of singlets: each of them is characterized by an experimental full linewidth Γ_i and an intensity β_i. In a second step (Sec. III C) the experimental linewidths are assumed and we tried to reproduce each spectrum with one site only as it has been done before: deviations between the preceeding experimental and the calculated β_i are observed and the singleness of the one-site solution is discussed in Sec. III D.

In Sec. III E, a new spectrum reproduction is suggested: it is based upon the superposition of two sites whose respective intensities vary at $T=13$ K. The linewidth Γ_i of each spectrum does not vary with it and the corresponding experimental β_i is equal to the calculated one.

B. Decomposition into singlets

The n peaks are considered as independent of each other in a given spectrum ($n=8$ at $T<13$ K and $n=6$ at $T>13$ K). The so-obtained reproductions of the spectra are characterized by a very minimum mean quadratic error.

Figure 2 shows the variation with T of Γ_{ex} and the

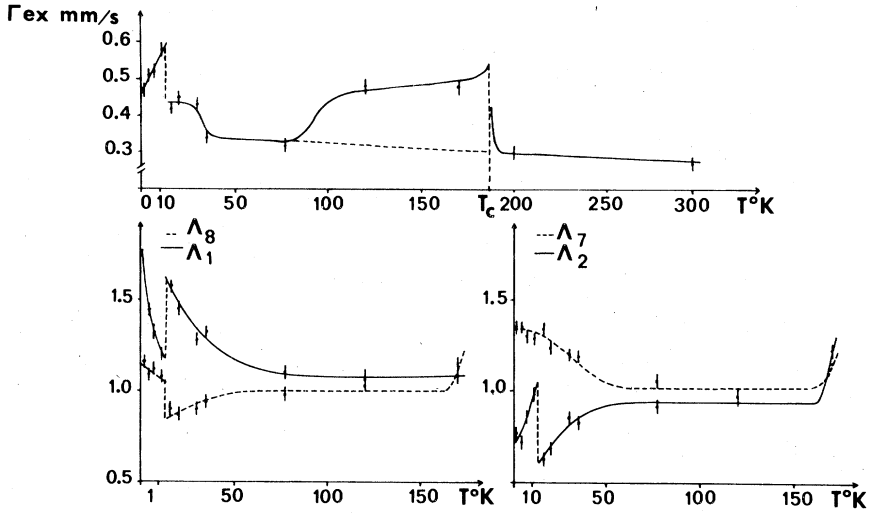

FIG. 2. Variation with temperature of the mean linewidth Γ_{ex} and of the broadening factors ν_i [Λ_i on the figure] related to the most intense peaks ($i=1$ and 8; 2 and 7).

ν_i related to the most intense peaks ($i=1$ and 8; 2 and 7): Γ_{ex} is characterized by two discontinuities, at T_C and at $T=13$ K. Furthermore, the plot for Γ_{ex} vs T for $T=35$, 77, 200, and 296 K gives a straight line. This linear part of the Γ_{ex} variation reflects its increase when T decreases. This comes from the fact that the f' factor is linearly increasing in this temperature region and is simulated by an increase of ν_a at t constant. At $T=120$ and 170 K, the Γ_{ex} broadening is not due to any instrumental ground.[19] It can be shown[19] that its origin cannot be due to a temperature inhomogeneity coming from the rilsan powder. Moreover, Fig. 2 shows that the Γ_{ex} discontinuity at $T=13$ K is associated with discontinuities of the broadening factors ν_1, ν_2, and ν_8.

C. One-site solution

In this approach, the experimental broadening factors ν_i and intensities β_i, as they have been deduced by the preceding decomposition into singlets, have been assumed in the runs: the mean quadratic error of spectra is slightly greater than the preceding one. The calculated positions of the peaks are in agreement with the experimental one as they have been deduced from the decomposition into singlets.

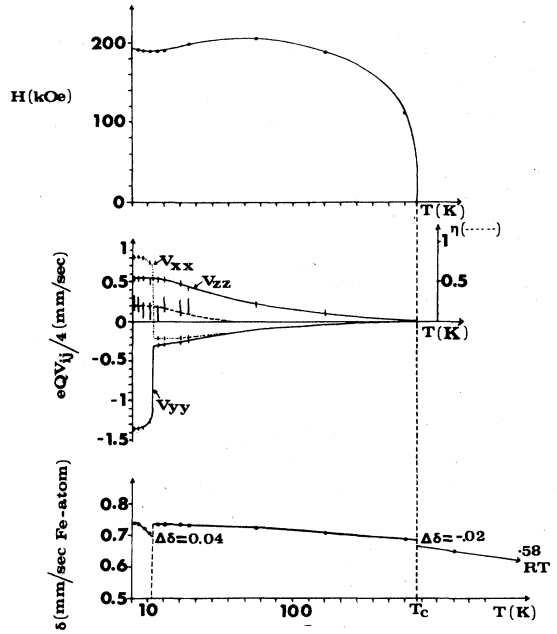

FIG. 3. Variations of the hyperfine magnetic field H, the barycenter δ of the $FeCr_2S_4$ spectra, and of the EFG (V_{ij} and η) in a single-site solution characterized by $\theta \sim \frac{1}{2}\pi$ at $T<13$ K and $\theta \sim 0$ at $T>13$ K. (V_{zz} represents the component of the EFG directed along H and not its principal component at $T<13$ K).

Figure 3 shows the variations of the hyperfine parameters with temperature: from these values, the program computes the calculated β_i values. They are not in agreement with the corresponding experimental values for the first peak at $T \lesssim 60$ K and for the second one at $T<13$ K. These results agree with those of Spender and Morrish[4] which showed also no discontinuity of H at 13 K, only a slight increase at $T<13$ K. The variations of the components of the EFG are also in agreement with those reported by Van Diepen and Van Stapele,[5] but our results are more accurate. Particularly, the asymmetry of the EFG appears at $T \lesssim 60$ K. Furthermore, the phase transition at 13 K is associated with a discontinuity of the barycenter δ of the spectra; δ is known to be the sum of two terms: the isomer shift δ_{is} which is temperature independent and the second-order Doppler effect δE which reflects the evolution with temperature of the barycenter. Then this discontinuity could result in a temperature expansion of the crystal lattice: this leads to an expansion of the radial part of the s wave functions, and gives a decrease of the s charge density at the nucleus and consequently an increase of the isomer shift. In fact, recent x-ray measurements[42] between $T=4.2$ and 20 K conclude as to the absence of any distortion, dilation anomaly, or discontinuity in the variation of $\partial a/\partial T$ vs T. Therefore, the δ-barycenter discontinuity can only result from a modification of the phonon spectrum and then of the second-order Doppler effect. Moreover, δ shows at T_C another discontinuity related to the magnetic order.[43]

D. Uniqueness of the preceding one-site solution

Let us discuss the singleness of the single-site solution obtained with anomalous experimental variations of the nuclear transition probability β_i and of the linewidth of each peak. This solution is characterized by

(a) $V_{ZZ}>0$, $\theta \sim 0$, η and $\phi \sim 0$

at $T>13$ K and

(b) $V_{ZZ}<0$, $\theta \sim \frac{1}{2}\pi$, $\eta \sim 0.2$, and $\phi \sim 0$

at $T<13$ K.

At $T<13$ K, there is no doubt about the singleness of solution (b).

On the other hand, at $T>13$ K, the Kundig's diagrams[30] show the possibility of obtaining nearly the same peak's position and calculated intensities β_i with solution (a) as well as with $V_{ZZ}<0$, $\eta \sim 1$, θ and $\phi \sim \frac{1}{2}\pi$. This shows that the programming of Hoy *et al.*[28] is not in contradiction with other results previously mentioned.[2,4,5] We have performed such a reproduction of spectra for $16<T<77$ K in a

single-site solution with $\eta=1$ and $\theta=\phi=\frac{1}{2}\pi$. The mean quadratic error is roughly the same as this obtained with solution (a). This is not surprising since, as in the case of solution (a), the experimental linewidth and β_i values of each peak have been assigned.

E. Two-site solution

The results discussed above suggest the test of a two-site solution in which the β_i of each peak are, respectively, equal to the calculated one from the hyperfine parameters of each site. Likewise, the broadening factors ν_i are equal to each other inside each site. Thus, we have reproduced the experimental spectra by superposing two closely related sites in order to remove the anomalous experimental variations of the β_i and Γ_i parameters of the single-site solutions.

1. $T<13$ K

The two sites have closely related hyperfine parameters with $V_{ZZ}<0$; $\theta=\frac{1}{2}\pi$, and $\phi=0$ or $\frac{1}{2}\pi$ have been assumed but not η. In order to obtain a minimum of the mean quadratic error it has been necessary to assign different broadening factor ν_j values corresponding to different site linewidths Γ_j ($\Gamma_1/\Gamma_2=1.70\pm0.05$) given by

$$\Gamma_j=\Gamma_{ex}(1+\nu_a\nu_j)/(1+\nu_a)\ . \tag{3}$$

The minimum of the mean quadratic error is obtained for site intensities respectively equal to $\alpha_1=0.75$ and $\alpha_2=0.25$. Table I gives the hyperfine parameters corresponding to the calculated Mössbauer spectra of Fig. 4(a).[44]

TABLE I. Hyperfine parameters and respective intensities of the two-site reproduction of $FeCr_2S_4$ Mössbauer spectra at $T<13$ K. This solution is characterized by $\theta=\frac{1}{2}\pi$, $\phi=0$ for site 1 and $\theta=\phi=\frac{1}{2}\pi$ for site 2. Γ_{ex} has been obtained using relation (1) in the text. The broadening factors ν_j of relation (3) are, respectively, $\nu_1=2.1$ and $\nu_2=1.0$.

		T (K) (±0.2)			
	Site No.	1.3	4.2	7	11[a]
α	1	0.74	0.76	0.74	0.75
(±0.1)	2	0.26	0.24	0.26	0.25
δ (mm/sec)	1	0.724	0.725	0.711	0.709
(±0.015)	2	0.865	0.885	0.886	0.862
	δ_{mean}	0.760	0.764	0.756	0.747
H (kOe)	1	193.7	193.5	191.7	187.9
(±0.5)	2	183.2	183.9	182.2	176.9
	H_{mean}	191.0	191.2	189.2	185.1
$\epsilon=eQV_{ZZ}/4$ (mm/sec)	1	−1.29(5)	−1.31(5)	−1.30	−1.23(5)
(±0.01)	2	−1.35	−1.33	−1.29	−1.26(5)
	ϵ_{mean}	−1.31	−1.32	−1.30	−1.24
η	1	0 31	0.29	0.26	0.24
(±0.1)	2	0.11	0.13	0.17	0.21
	η_{mean}	0.26	0.25	0.24	0.23
Γ_{ex} (mm/sec) (±0.01)		0.30	0.31	0.32	0.38
Γ_1/Γ_2		1.65	1.66	1.68	1.75

[a]For this temperature, intensities have been fixed during the runs.

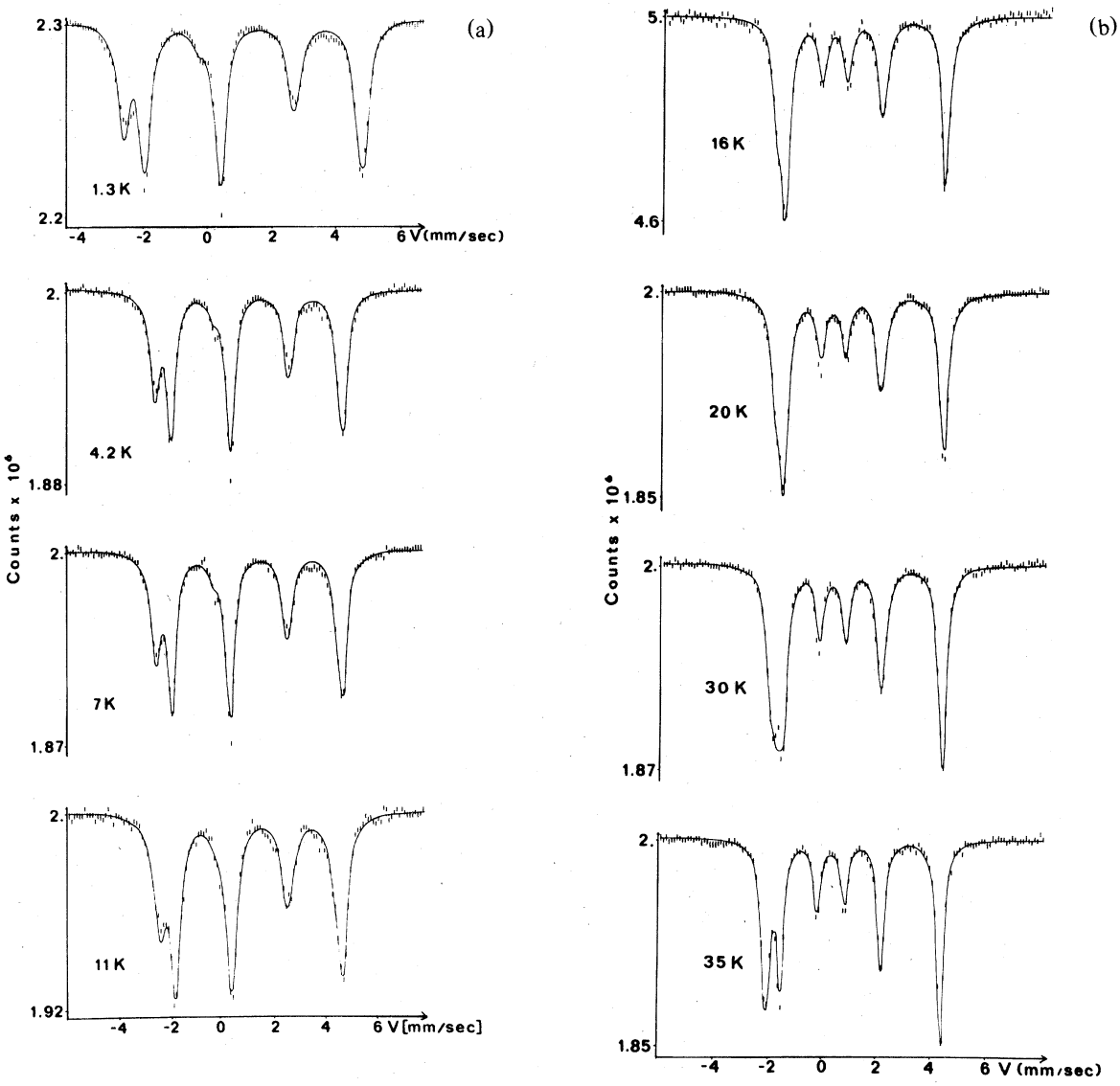

FIG. 4. Experimental points and two-site calculated reproduction of $FeCr_2S_4$ Mössbauer spectra corresponding to Table I [(a) $T < 13$ K] and Table II [(b) $T > 13$ K].

2. $T > 13$ K

The same peak's linewidth $\Gamma_{ex}(\nu_j = 1)$ has been used for the two sites which are characterized by

$$V_{ZZ} > 0, \quad \eta = 0, \quad \theta = \phi = 0 \quad \text{for } j = 1$$

and

$$V_{ZZ} < 0, \quad \eta = 1, \quad \theta = \phi = \tfrac{1}{2}\pi \quad \text{for } j = 2 .$$

These values of η, θ, and ϕ have been assigned in the program steps in order to leave a physical meaning to the reproduction and thus to avoid too many adjustable parameters. The mean quadratic errors are similar to the single-site-solution one. Table II gives the values of the hyperfine parameters of the two sites and their respective intensities, corresponding to the calculated spectra of Fig. 4(b). The fact that the sites have the same intensity α and isomer shift δ at a given temperature constitutes a remarkable trend. As at $T < 13$ K, Γ_{ex} varies like in the single-site solution but its experimental value is slightly reduced.

TABLE II. Hyperfine parameters and respective intensities in the two-site reproduction of $FeCr_2S_4$ Mössbauer spectra at $T > 13$ K. This solution is characterized by $V_{zz} > 0$, $\theta = \phi = 0$, $\eta = 0$ for site 1 and $V_{zz} < 0$, $\theta = \phi = \frac{1}{2}\pi$, $\eta = 1$ for site 2.

		T (K) (±0.2)				
	Sites	16	20	30[a]	35	77[a]
α	1	0.50	0.51	0.50	0.50	0.50
(±0.01)	2	0.50	0.49	0.50	0.50	0.50
δ (mm/sec)	1	0.760	0.763	0.766	0.749	0.734
(±0.015)	2	0.734	0.735	0.733	0.722	0.719
H (kOe)	1	183.9	184.8	191.1	198.0	204.6
(±0.5)	2	190.7	191.8	196.0	200.6	209.2
$eQV_{ZZ}/4$ (mm/sec)	1	0.57(5)	0.57	0.52	0.46	0.23
(±0.01)	2	−0.48(5)	−0.49	−0.44	−0.39	−0.19(5)
Γ_{ex} (mm/sec) (±0.01)		0.39	0.41	0.39	0.31	0.30

[a]For these temperatures, the intensities have been fixed during the runs.

3. *Discussion*

Figure 5 shows the variation of the hyperfine magnetic fields, barycenters, and principal components of the EFG of the preceding two sites, on both sides of 13 K: The main features are the following:

(a) Hyperfine fields show discontinuities at $T = 13$ K which were not found in all previous reproductions. These fittings were based on a single-site solution whose hyperfine magnetic field varies continuously on both sides of 13 K (site labeled 1 in Fig. 5).

(b) The two sites are characterized by two elementary spectra with different intensities, linewidths, and barycenters at $T < 13$ K, while they are the same above 13 K. Nevertheless the mean barycenter at $T < 13$ K is the same as at $T > 13$ K. This agrees with the properties of the second-order phase transition which is not of crystallographic nature but of magnetic nature. This suggests that the apparition of two different barycenters at $T < 13$ K is not due to a modification of the isomer shift but comes from two different couplings between the electronic system and the phonon spectrum resulting in two different second-order Doppler effects at $T < 13$ K.

(c) At $T < 13$ K, the intensity of the site is the greater (0.75), the larger is the linewidth, the greater is the hyperfine field, and the lower the barycenter. This indicates that a stronger coupling of the electronic system with crystalline vibrations leads to a greater decrease of the barycenter by the second-order Doppler effect δE.

IV. INTERPRETATION

Since crystal-field theory fails to explain the temperature variations of the hyperfine parameters of

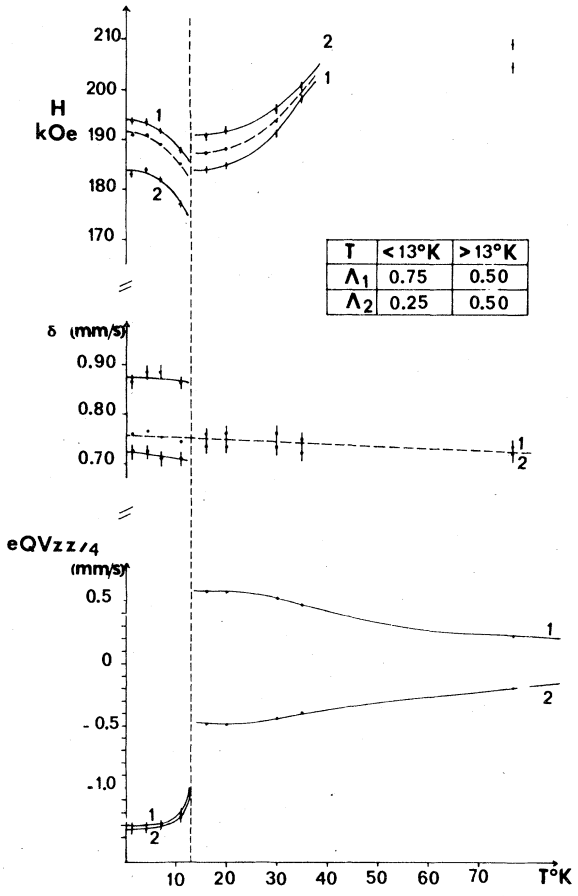

FIG. 5. Variation with T of the hyperfine magnetic fields, barycenters, and principal components of the EFG of the two sites used in the reproduction of Mössbauer spectra. Dashed lines show the variation of the mean averaged values of H and δ.

$FeCr_2S_4$ Mössbauer spectra, it enables us to describe the d electrons of A-site Fe^{2+} as itinerant instead of localized. Following Mott,[45] the main interaction which leads to localized d electrons in the transition-metal compounds is U, the potential energy arising from the intra-atomic electronic repulsion. The first theoretical approach for correlations in narrow bands is due to Hubbard for s and d electrons.[46]

Our interpretation can be based upon the assumption describing the sixth $3d$ electron of A-site Fe^{2+} in a narrow and hybridized band. Goodenough[47] has pointed out the delocalization tendency of the sixth $3d$ electron of A-site Fe^{2+}: the B-site excited Cr^{2+} state is close in energy to the sixth-$3d$-electron narrow band of A-site Fe^{2+} and electronic transfers are possible — real or virtual. Figure 6(a) shows at $T > T_C$ the band structure of $FeCr_2S_4$ in relation to the p-type semiconducting properties of the compound.

A. At $T > 13$ K

The sixth $3d$ electron occupies the orbitals derived from the base (ϵ, θ) of the E representation of the T_d group. The first one, usually written

$$|\epsilon\rangle = \frac{1}{2^{1/2}}(|2\rangle + |-2\rangle) ,$$

has x^2-y^2 symmetry and leads to $V_{ZZ} > 0$, $\eta = 0$, and $\theta = \phi = 0$. The second one is supposed to have mainly $3z^2-r^2$ symmetry and leads to $V_{ZZ} < 0$ like $|\theta\rangle = |0\rangle$. But we assume that this orbital is hybridized with the B-site Cr^{2+} excited state, the hybridization being such that $\eta = 1$ and $\theta = \phi = \frac{1}{2}\pi$.

The sixth $3d$ electron of A-site Fe^{2+} occupies indifferently these two orbitals leading to the equal-intensity Mössbauer sites referred to, respectively, by the numbers 1 and 2 (Table II). This situation is characteristic of an orbital paramagnetism with an equal probability of having the sixth $3d$ electron of Fe^{2+} either in the first orbital or in the second one (Fig. 6(b)]:

(a) at $T > T_C$, the relaxation frequency ω_{hop} of this electron between the two orbitals is fast compared with $2\epsilon/\hbar$, so that a singlet is observed $[\epsilon = \frac{1}{4}(eQV_{zz}]$.

(b) at $T \lesssim T_C$, an EFG is induced by the magnetic order since the relaxation frequency ω_{hop} decreases with temperature so that $\omega_{hop} < 2\epsilon/\hbar$ and $\omega_{hop} < \omega_L$, where ω_L is the nuclear Larmor precession frequency.

Further deductions can be made from the spectra programming at $T > T_C$: the overlap of the hybridized $3z^2-r^2$ orbital with the anion s and p orbitals is greater than that of the corresponding x^2-y^2 orbital. Then, when the sixth $3d$ electron of A-site Fe^{2+} occupies the hybridized $3z^2-r^2$ orbital the value of the corresponding $|V_{ZZ}|$ is lower than the $|V_{ZZ}|$ value obtained when the x^2-y^2 orbital is occupied. This reduction comes from the increase of the covalency parameter α^2 which affects the $\langle r^{-3}\rangle_{3d}$ value

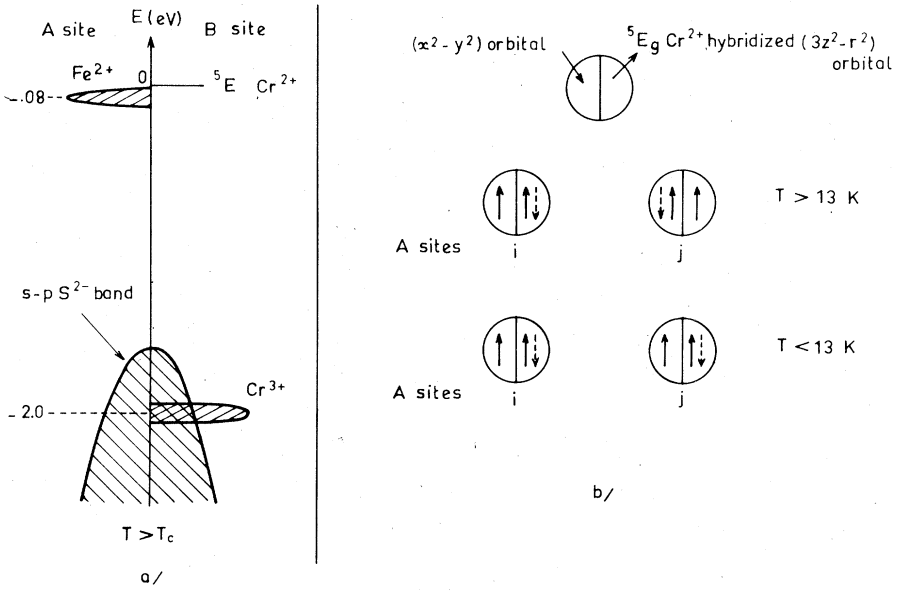

FIG. 6. (a) Single-electron narrow-band scheme for $FeCr_2S_4$ at $T > T_C$. (b) Occupation of x^2-y^2 and hybridized $3z^2-r^2$ orbital by the sixth $3d$ electron (dashed lines) for A sites i and j with temperature.

of the usual formula[21]

$$V_{ZZ} = \frac{2}{21}|e|\langle r^{-3}\rangle_{3d}[3L_Z^2 - L(L+1)] ,$$

$$\langle r^{-3}\rangle_{3d} = (1-\alpha^2)\langle r^{-3}\rangle_0 ,$$

where the label zero refers to the free ion.

This also explains the tendency — but not very significant — to observe an isomer shift δ_2 slightly lower than δ_1 (cf. Table II), the indexes 1 and 2 referring to the x^2-y^2 and the hybridized $3z^2-r^2$ orbital.

This covalency effect must affect in the same manner the hyperfine field H_2: if this reduction of H_2 with respect to H_1 is estimated to be ~ 5 kOe, then a further increase of ~ 15 kOe of H_2 with respect to H_1 is necessary to explain the experimental observation ($H_2 - H_1 \sim 10$ kOe). This increase of ~ 15 kOe of H_2 must probably result from a supertransferred hyperfine magnetic field due to the chromium ions. This seems plausible since it is the $3z^2-r^2$ orbital which has been supposed to be hybridized with the B-site Cr^{2+} state.

B. At $T < 13$ K

Both sites are now characterized by $V_{ZZ} < 0$, $\eta \sim 0.2$, and $\theta = \frac{1}{2}\pi$. Then the sixth $3d$ electron of A-site Fe^{2+} occupies only the $3z^2-r^2$ hybridized orbital [Fig. 6(b)], but the second-order phase transition at $T = 13$ K is associated with a reduction of the hybridization of this orbital with the B-site Cr^{2+} state, since $\eta \sim 0.2$ at $T < 13$ K instead of $\eta = 1$ at $T > 13$ K. By analogy with the orbital antiferromagnetism described by Cyrot *et al.*,[6] this situation can be called a ferromagnetic orbital ordering since the sixth $3d$ electron of A-site Fe^{2+} occupies the same orbital for all the sites. This transition from an orbital paramagnetism to an orbital ferromagnetic order occurs at a temperature lower than T_C. It is to our knowledge the first experimental evidence of such a second-order phase transition.

The two sites are, respectively, characterized by $\phi_1 = 0$ (site 1) and $\phi_2 = \frac{1}{2}\pi$, where ϕ is the polar angle associated to the azimuthal angle θ (cf. Table I). Since the spins are always directed along the x direction, this means that a slow relaxation mechanism affects the V_{XX} and V_{YY} principal component of the EFG: more precisely, this relaxation is such that the X and Y axes are flipping within time from $\pm\frac{1}{2}\pi$ around the Z principal axis which stays perpendicular to the spin direction ($\theta = \frac{1}{2}\pi$). Moreover, the X principal axis spend $\alpha_1 = 75\%$ of the time in the x direction ($\phi_1 = 0$) against $\alpha_2 = 25\%$ for the Y principal axis ($\phi_2 = \frac{1}{2}\pi$). This is associated with a linewidth Γ_1 larger than Γ_2 ($\Gamma_1/\Gamma_2 \sim 1.70$). This EFG slow relaxation is related with two different couplings of the electronic band with the phonon spectrum according to whether $\phi_1 = 0$ or $\phi_2 = \frac{1}{2}\pi$.

The second-order Doppler effect results at the temperature T from the zero energy and from the thermal agitation. It is proportional to the mean quadratic velocity $\langle v^2\rangle$ of the nucleus. Then, the strongest coupling of the band with lattice vibrations which leads to the greater decrease of the spectra barycenter by second-order Doppler effect is related to different values of $\langle v^2\rangle$ according to whether $\phi_1 = 0$ or $\phi_2 = \frac{1}{2}\pi$. In other words it means that the mean quadratic velocity $\langle v^2\rangle$ of the nucleus is greater when the X principal axis is directed along the x direction ($\phi_1 = 0$) than when $\phi_2 = \frac{1}{2}\pi$. This should have some consequences on the values of the mean quadratic displacements $\langle x^2\rangle$ of the nucleus and thus on the Mössbauer-factor f' values of the two sites. It should be pointed out that the present description does not take into account such differences between the two site f' values since the same f' factor has been used during the runs.

Finally, these different couplings of the band with the phonon spectrum act also on the hyperfine field H and to a less extent on the V_{ZZ} values of the two sites: at $T = 0$, the $\frac{1}{4}(eQV_{ZZ})$ values of the two sites are, respectively, $\epsilon_1 = -1.30$ and $\epsilon_2 = -1.35$ mm/sec. Compared to the theoretical value -1.5 mm/sec, these values are reduced by a factor $q = 0.87$ and 0.90. Taking into account the additional reduction of V_{ZZ} by covalency, these q values are to be corrected and are probably closer to unity. This seems to agree with a reduction of V_{ZZ} by a linear and weak dynamic Jahn-Teller effect[34] as it acts on the ^5E orbital doublet of T_d-symmetry Fe^{2+} and leads to a fundamental vibronic doublet. It can be assumed that such an effect acts in a similar fashion in the present case of a narrow band by analogy with classical band calculations.[48,49] But in this case, an analogous reduction of the hyperfine fields ($H_1 < H_2$) should be observed, contrary to present experimental results ($H_1 > H_2$).

Then we suggest that the coupling of the hybridized narrow band with the phonon spectrum at $T < 13$ K is quite different from a classical linear and weak dynamic Jahn-Teller effect.

V. CONCLUSION

The electric and magnetic properties as well as the Mössbauer spectra of polycrystalline stoichiometric $FeCr_2S_4$ are hence well understood on the basis of a single-electron narrow band of the sixth $3d$ electron of the Fe^{2+} ion. This electron occupies two orbitals, the x^2-y^2 one and the $3z^2-r^2$ one which is hybridized with the B-site Cr^{2+} state. This model seems to be more adequate to explain the linewidth and the intensity irregularities of the Mössbauer spectra than the single-ion crystal-field theory which explains sat-

isfactorily the A-site diluted Fe^{2+} thiospinel Mössbauer spectra. Moreover, the crystal-field theory assumes that the $3d$ electrons are localized. In our case they are responsible for the magnetic and for the low-mobility p-type transport properties of $FeCr_2S_4$.

It is suggested that the second-order phase transition at $T = 13$ K is related to a magnetic transformation characterized by an orbital paramagnetism at $T > 13$ K and an orbital ferromagnetic order at $T < 13$ K. This transition is associated with the appearance at $T < 13$ K of a slow relaxation of the X and Y principal axis of the EFG around the Z axis which is perpendicular to the spin direction. It is also related to a new type of coupling of the band with the phonon spectrum at $T < 13$ K. This coupling is quite different from a linear and weak dynamic Jahn-Teller effect as is the case for the A-site dilute Fe^{2+}.

ACKNOWLEDGMENTS

The authors wish to express their thanks to Professor J. Friedel for helpful discussions concerning the A-site-Fe^{2+} sixth-$3d$-electron narrow-band hybridization with the B-site Cr^{2+} state. They are indebted to Dr. M. Cyrot for discussions on the orbital para-ferromagnetic-order transition. They are also grateful to Dr. P. Imbert and H. Oudet for discussions related, respectively, to singlets decomposition of spectra and to crystal-field theory. Special gratitude is due to Dr. Winterberger for neutron-diffraction measurements and to Dr. F. Sayetat for low-temperature x-ray data. This paper is based on a thesis submitted by L. Brossard for the "Docteur-ès-Sciences" degree at the Faculty of Sciences of Paris Sud, July 1977.

[1]F. K. Lotgering, Philips Res. Rep. 11, 190 (1956).
[2]M. Eibschutz, S. Shtrikman, and Y. Tenenbaum, Phys. Lett. A 24, 563 (1967).
[3]F. K. Lotgering, A. M. Van Diepen, and J. F. Olijhoek, Solid State Commun. 17, 1149 (1975).
[4]M. R. Spender and A. H. Morrish, Solid State Commun. 11, 1417 (1972).
[5]A. M. Van Diepen and R. P. Van Stapele, Solid State Commun. 13, 1651 (1973).
[6]M. Cyrot and C. Lyon-Caen, J. Phys. (Paris) 36, 253 (1975); J. Phys. (Paris) 37, C4-183 (1976).
[7]R. J. Bouchard, P. A. Russo, and A. Wold, Inorg. Chem. 4, 685 (1965).
[8]G. Shirane, D. E. Cox, and S. J. Pickart, J. Appl. Phys. 35, 954 (1964).
[9]P. Gibart, J. L. Dormann, and Y. Pellerin, Phys. Status Solidi 36, 187 (1967).
[10]P. Gibart, L. Goldstein, and L. Brossard, J. Magn. Magn. Mater. 3, 109 (1976).
[11]G. L. Bacchela, P. Imbert, P. Meriel, E. Martel, and M. Pinot, Soc. Sci. Bretagne 39, 121 (1965).
[12]G. Haacke and L. C. Beegle, Phys. Rev. Lett. 17, 427 (1966).
[13]P. Gibart, A. Begouen-Demeaux, C.R.A.S. 268C, 816 (1969); L. Goldstein, P. Gibart, C.R.A.S. 269B, 471 (1969); L. Goldstein, State thesis (Orsay, 1974) (unpublished).
[14]T. Watanabe, I. Nakada, Technical Report of I.S.P.A. 831 (1977) (unpublished).
[15]M. Heritier, State thesis (Orsay, 1975) (unpublished).
[16]R. P. Van Stapele, J. S. Van Wieringen, and P. F. Bongers, J. Phys. (Paris) 32, C1-53 (1971).
[17]L. Goldstein, P. Gibart, L. Brossard, in *Proceedings of the 21st Conference on Magnetism and Magnetic Materials, Philadelphia, 1975,* edited by J. J. Becker, G. H. Lander, and J. J. Rhyne, AIP Conf. No. 29 (AIP, New York, 1976), p. 405.
[18]The simple Néel structure has been recently verified at $T = 4.2$ and 27 K by Dr. Winterberger at Grenoble (private communication).
[19]L. Brossard, State thesis (Orsay, 1977) (unpublished).
[20]L. Brossard, L. Goldstein, P. Gibart, and J. L. Dormann, J. Phys. Chem. Solids (to be published).
[21]A. Abragam and B. Bleaney, *Electron paramagnetic resonance of transition ions* (Clarendon, Oxford, 1970), p. 695.
[22]B. Hoekstra, R. P. Van Stapele, and A. B. Voermans, Phys. Rev. B 6, 2762 (1972).
[23]A. M. Van Diepen and R. P. Van Stapele, Phys. Rev. B 5, 2462 (1972).
[24]U. Ganiel, M. Kestigian, and S. Shtrikman, Phys. Lett. A 24, 577 (1967); J. Appl. Phys. 39, 1254 (1968).
[25]U. Ganiel and S. Shtrikman, Phys. Rev. 167, 258 (1968).
[26]H. Oudet, L. Brossard, J. L. Dormann, P. Gibart, and L. Goldstein, J. Phys. (Paris) 40, C2-258 (1979).
[27]F. Hartmann Boutron, J. Phys. 29, 212 (1968).
[28]G. R. Hoy and S. Chandra, J. Chem. Phys. 47, 961 (1967); G. R. Hoy and K. P. Singh, Phys. Rev. 172, 514 (1968); G. R. Hoy, K. P. Singh, and S. Chandra, *Hyperfine structure and nuclear radiations* (North-Holland, Amsterdam, 1968), p. 516.
[29]M. R. Spender and A. H. Morrish, Can. J. Phys. 50, 1125 (1972).
[30]W. Kundig, Nucl. Instrum. Methods F 4, 219 (1967).
[31]J. A. Tjon and M. Blume, Phys. Rev. 165, 456 (1968).
[32]J. R. Regnard and J. Chappert, J. Phys. (Paris) 37, C6-611 (1976).
[33]C. Garcin, P. Imbert and G. Jehanno, Solid State Commun. 21, 545 (1977).
[34]F. S. Ham, J. Phys. (Paris) 35, C6-121 (1974).
[35]F. S. Ham, *Jahn Teller effects in E.P.R. Spectra-Electron Paramagnetic Resonance,* edited by S. Geschwind (Plenum, New York, 1972).
[36]M. C. M. O'Brien, Proc. R. Soc. London Sect. A 281, 323 (1964).
[37]F. S. Ham, Phys. Rev. 166, 307 (1968).
[38]F. Hartmann-Boutron and P. Imbert, J. Appl. Phys. 39, 775 (1968).

[39]A. Gerard, P. Imbert, H. Prange, F. Varret, and M. Wintenberger, J. Phys. Chem. Solids 32, 2091 (1971).
[40]J. L. Dormann, L. Brossard, and G. A. Fatseas, Internal Report of Magnetism Laboratory, Bellevue (1972) (unpublished).
[41]W. M. Wisscher, unpublished results cited by D. A. Shirley, M. Kaplan, and P. Axel, Phys. Rev. 123, 816 (1961).
[42]X-rays measurements have been done by Dr. F. Sayetat at Grenoble (private communication).
[43]S. Alexander and D. Treves, Phys. Lett. 20, 134 (1966).
[44]The spectrum at $T=1.3$ K has been done at Dr. Imbert's group, at Saclay.
[45]N. F. Mott and Z. Zinamon, Rep. Prog. Phys. 33, 881(1970).
[46]J. Hubbard, Proc. R. Soc. London Sect. A 276, 238 (1963); A 277, 237 (1964).
[47]J. B. Goodenough, J. Phys. Chem. Solids 30, 261 (1969).
[48]R. Englman, *The Jahn-Teller effect in molecules and crystals* (Interscience, New York, 1972).
[49]T. P. Das, Physica Scripta 11, 121 (1975).